

93-12

REPORT

CRF

S DTIC ELECTE D
A OCT 12 1993

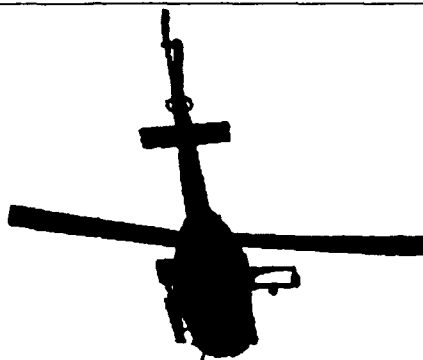
2



Footprint Size of a Helicopter-Borne Electromagnetic Induction Sounding System Versus Antenna Altitude

Austin Kovacs, J. Scott Holladay and Clyde J. Bergeron, Jr.

July 1993



This document has been approved for public release and sale; its distribution is unlimited.

AD-A270 468



93-23894



APR



93 10 8 105

Abstract

Helicopter-towed electromagnetic induction sounding systems have recently been used for the remote measurement of sea-ice thickness and shallow sea bathymetry. An inherent aspect of this sensing technology is the large area, the footprint, over which an individual sounding is made. This report gives an overview of previous footprint size assessments and presents new footprint size estimates determined from sea ice survey data and analytical calculations. All footprint determinations were found to be in reasonable agreement. For a vertical coaxial coil antenna arrangement the apparent footprint diameter was found to be about 1.25 times the antenna height above the conductive surface, and for a horizontal coplanar coil configuration the ratio is about 3.75 times the antenna height.

For conversion of SI metric units to U.S./British customary units of measurement consult ASTM Standard E380-89a, *Standard Practice for Use of the International System of Units*, published by the American Society for Testing and Materials, 1916 Race St., Philadelphia, Pa. 19103.



**US Army Corps
of Engineers**

Cold Regions Research &
Engineering Laboratory

Footprint Size of a Helicopter-Borne Electromagnetic Induction Sounding System Versus Antenna Altitude

Austin Kovacs, J. Scott Holladay and Clyde J. Bergeron, Jr.

July 1993

Accession For	
NTIS CRA&I	<input checked="" type="checkbox"/>
DTIC TAB	<input type="checkbox"/>
Unannounced	<input type="checkbox"/>
Justification	
By	
Distribution /	
Availability Codes	
Dist	Avail and/or Special
A-1	

Prepared for
NAVAL RESEARCH LABORATORY
and
U.S. COAST GUARD

DTIC QUALITY INSPECTED

PREFACE

This report was prepared by Austin Kovacs, Research Civil Engineer, U.S. Army Cold Regions Research and Engineering Laboratory; J. Scott Holladay, Geonex-Aerodat, Inc., Mississauga, Ontario, Canada; and Clyde J. Bergeron, Jr., University of New Orleans, New Orleans, Louisiana.

Funding for this study was provided by the Naval Research Laboratory, under contract N6845286MP6003 and by the U.S. Coast Guard under contract DTICG23-92-F-HNF062-2.

The authors acknowledge the helpful review of this report by Professor Juliette Ioup of the Department of Physics and Geophysical Research Laboratory, University of New Orleans, Louisiana, and Professor Alexander Becker, Department of Materials Science, of the University of California, Berkeley. The authors also wish to acknowledge the field assistance of Rexford M. Morey, of Morey Research Company; James Lee, Ian R. St. John, and Gregory Luus of Geonex-Aerodat, Inc.; Deborah Diemand, John Kalafut and John Bayer of CRREL; and the data processing assistance of John Bement at CRREL.

The contents of this report are not to be used for advertising or promotional purposes. Citation of brand names does not constitute an official endorsement or approval of the use of such commercial products.

CONTENTS

	Page
Preface	ii
Introduction	1
Transmitted field shape	2
HEM footprint size	4
Conclusions	11
References	12
Abstract	13

ILLUSTRATIONS

Figure

1. Three typical HEM system coil arrangements	2
2. Primary electromagnetic field direction for two transmitters	2
3. Idealized surfacial electric current pattern	3
4. Representative surfacial current density profile	3
5. Representative surfacial current density profile along AA' and BB'	4
6. Estimated surfacial current density contribution at 30-m elevation for coaxial and a coplanar HEM antenna coil orientation vs. idealized square foot-coaxial print width-to-antenna height ratio	4
7. Measured response of a coaxial HEM system flown from over thick first-year sea ice out over a lead with thin ice and from the thin lead ice back over the thicker first-year sea ice	5
8. Measured response of a coaxial HEM system as it was flown from over thick first-year sea ice out over thin lead ice and then back over first-year sea ice	6
9. Ice thickness distribution along the 1990 and 1991 survey lines	6
10. HEM determined vs. drillhole-measured ice thickness along the 1990 survey line	7
11. Autocorrelation function of ice thickness vs. lag distance for drillhole- measured and HEM-determined ice thickness along the 1990 survey line	8
12. HEM-determined vs. drillhole-measured ice thickness along the 1991 survey line	9
13. Maximum HEM-determined pressure ridge ice thickness vs. bird elevation above the surface	9
14. Autocorrelation function of ice thickness vs. lag distance for drillhole- measured and HEM-determined ice thickness along the 1991 survey line	10

Footprint Size of a Helicopter-Borne Electromagnetic Induction Sounding System Versus Antenna Altitude

AUSTIN KOVACS, J. SCOTT HOLLADAY AND CLYDE J. BERGERON, JR.

INTRODUCTION

Ice covers large areas of the Arctic and Antarctic seas. The thickness and distribution of this veneer are of considerable importance for efficient ship routing, design of offshore structures, and scientific sea ice dynamic-thermodynamic studies. Before 1985, many techniques were evaluated for the remote measurement of sea-ice thickness. Most met with limited success because of losses associated with the high brine inclusion content and related high conductivity of sea ice.

In 1985, a conventional helicopter-towed geophysical four-frequency electromagnetic (EM) induction sounding system was first used to estimate sea-ice thickness (Kovacs et al. 1987). The EM sounding system works according to the principles of electromagnetic induction, where the electromagnetic fields are governed by diffusion rather than a wave equation. A transmitter coil is excited by a sinusoidal electric current. This produces an alternating magnetic field in space so that electromagnetic currents are induced in any nearby conductors (e.g., seawater). These induced currents in turn produce a secondary magnetic field that is sensed by the receiver coil.

Located halfway between the transmit and the receiver antenna coils is a "bucking coil." At this location the primary field is about eight times stronger than at the receiver coil, but the secondary field is essentially the same. Therefore, the bucking coil is designed to have eight times less effective area than the receiver coil so that simple subtraction of the received signal at the bucking coil from the received signal at the receiver coil "bucks out" the primary field's, leaving a slightly attenuated secondary component. Using this technique, the secondary field can be measured with high precision; its in-phase and quadrature components are recorded digitally in

parts per million (ppm) of the primary magnetic field with a precision of about 1 ppm. These data are used to determine the height of the antenna housing (bird) above the seawater surface and its conductivity. At the same time the bird's altitude above the ice surface is measured by a laser altimeter. Thus the apparent pack-ice thickness is obtained simply from the difference in these two distances.

The 1985 EM sounding field trials, made over the winter Beaufort Sea ice, were encouraging. Further EM system refinements led to halving the towed sensor platform length from about 6.5 to 3.5 m (Kovacs and Holladay 1990) and then to the development in 1990 of a wideband system having a frequency range from about 5 to 200 kHz and the unique capability to process the data, using a one-dimensional layered-halfspace inversion routine, and display the ice thickness in real time at >10 Hz. At the inception of this EM test and evaluation program, a persistent question was: How large was the area over which an integrated ice thickness measurement was made? For the purpose of this discussion, the basic unit of resolution will be called the footprint. This will be loosely defined as the horizontal distance along a survey line from which 90% of the ground response of the system arises. General rule-of-thumb estimates that were available in the geophysical community in 1985 gave the footprint of a helicopter-towed electromagnetic (HEM) induction sounding system as being about 2 to 3 times the antenna height above, for example, a conductive seawater surface. The size of the footprint is important to understanding the degree to which HEM sounding spatially smoothes out the undulating seawater relief associated with ice thickness variations. In short, a large footprint will tend to smooth or subdue the thickness of pressure ridge keels and ice relief that has a width on the order of the sounding system's footprint or smaller. In this

report we present recent assessments of the HEM footprint size.

TRANSMITTED FIELD SHAPE

A HEM system's antenna housing (bird) is generally suspended about 30 to 40 m below the helicopter and is towed about 20 to 30 m above the surface. Inside the cigar-shaped bird are circular coil pairs (a transmit Tx coil and a receiver Rx coil). The coil pairs are generally arranged as shown in Figure 1, with a bucking coil located in the same orientation halfway

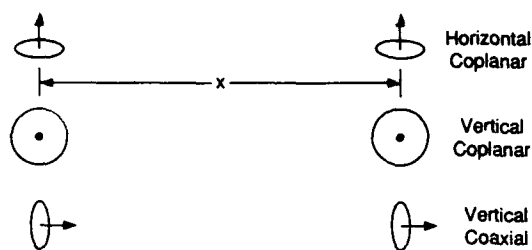


Figure 1. Three typical HEM system coil arrangements. Arrows indicate the magnetic dipole orientation (from Kovacs et al. 1987).

between them. The direction (but not the magnitude) of the magnetic field lines generated by the coaxial and horizontal coplanar transmitter is shown in Figure 2. In these diagrams the bird axis is horizontal. The vertical coplanar coil configuration generates a field distribution identical to that of the coaxial coil but rotated 90° into the page. A more important aspect of the effect of coil configuration used in sea ice sounding is the pattern of the currents induced in the seawater by the Tx coil, because it is these induced currents that generate the signal measured and analyzed by the HEM system. The zone in which the strongest current flow occurs will be the region that contributes most to the response measured by the HEM system. Therefore, the smaller the area of high current flow the smaller the footprint.

The model used by Liu (1989) to calculate the surface current distributions shown in Figure 3 was a highly conducting sheet whose effective depth depends on the frequency. The angles of the arrows indicate the directions of the currents, while their length denotes the relative strength of the current at that position. At high frequencies (>10 kHz), these currents lie close to the seawater surface and, since their distance from the antenna coil can be estimated

accurately, the use of high frequencies permits an accurate estimate of the antenna altitude above the water surface. At lower frequencies, this pattern becomes more diffuse and is centered at a greater depth beneath the water surface. This is why there is better (deeper) bathymetric sampling by a system operating at lower frequencies, e.g., at 50 Hz. A strong concentration of current located immediately below the transmitter (at x and $y = 0$) is shown in Figure 3a. Here the zone of maximum current strength lies in an ellipse with its short axis lying along the bird axis (x -direction) and its long axis perpendicular to the bird axis (y -direction). Two zones of weak response precede and follow the bird along its axis. The bird height assumed for this diagram and the next was 30 m.

The induced surface currents, as calculated by Liu (1989), for the horizontal coplanar transmitter mode are shown in Figure 3b. In this configuration, the currents are strongest in a ring with a radius of about two-thirds the flight height. Directly below the transmitter there is a narrow zone of zero response. The response dies off sharply

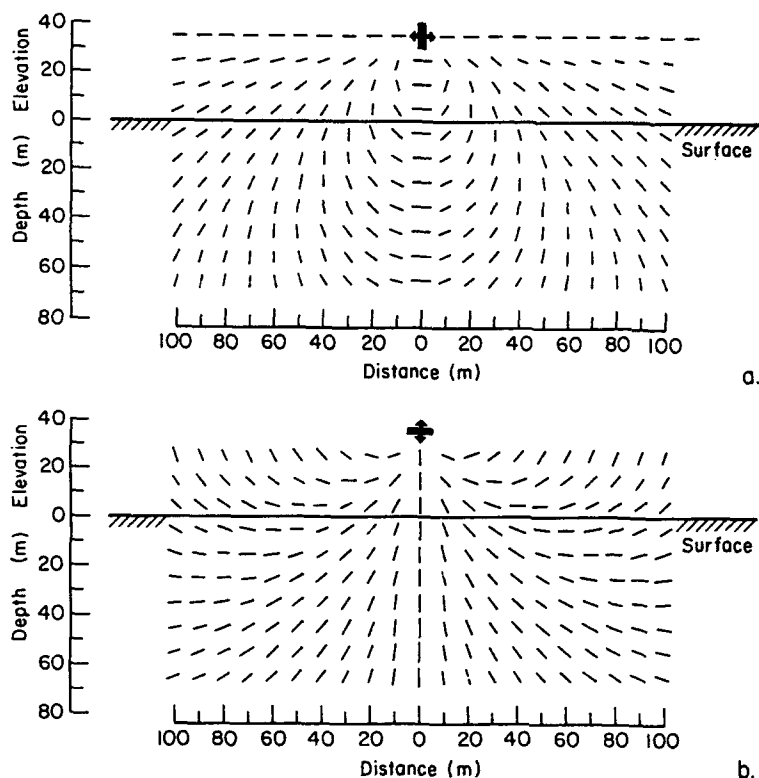


Figure 2. Primary electromagnetic field direction for two transmitters. Arrows indicate the magnetic dipole antenna orientations (from Kovacs et al. 1987).

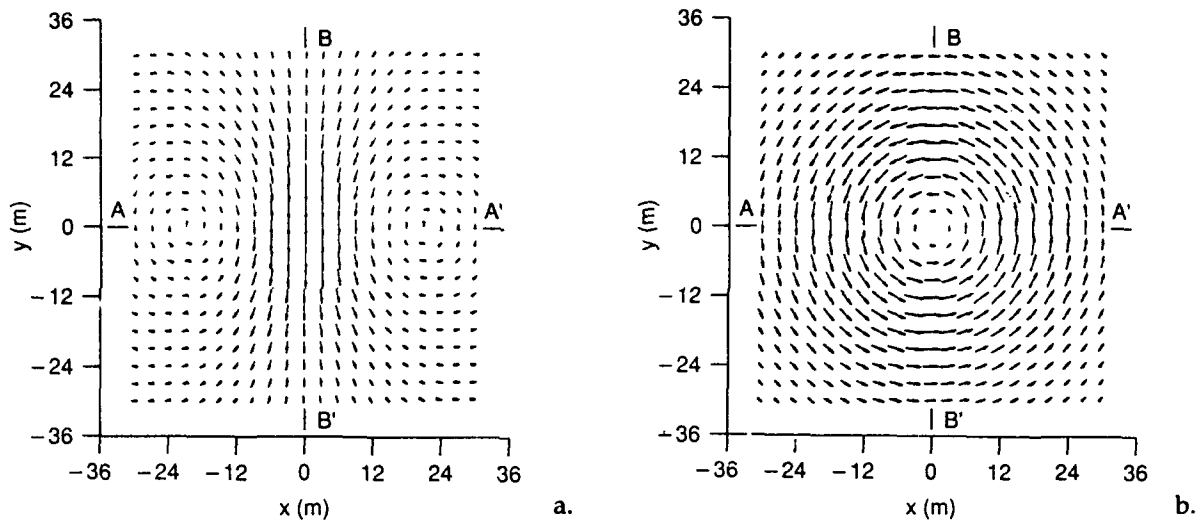
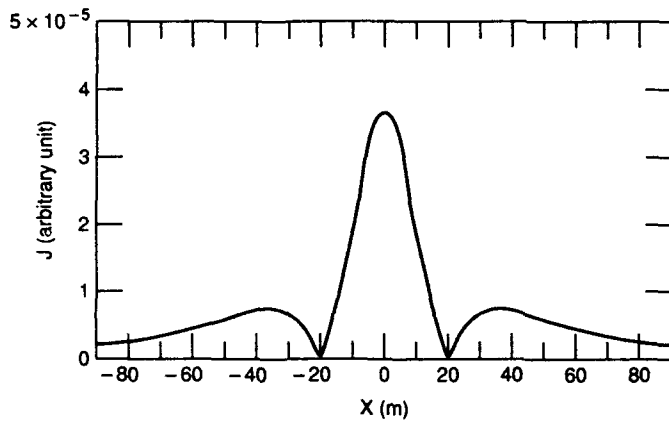
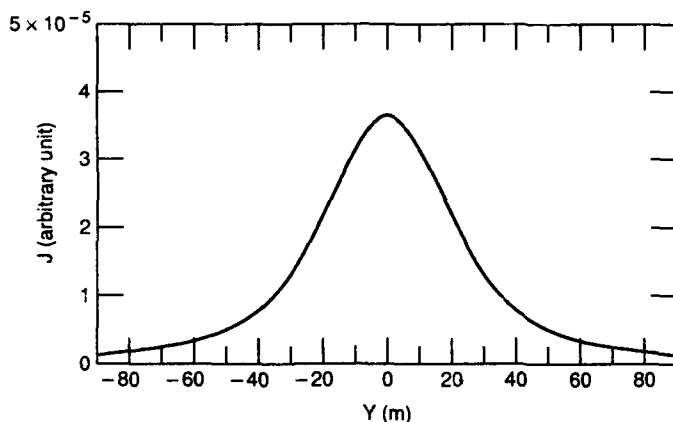


Figure 3. Idealized surfacial electric current pattern (from Liu 1989).



a. Along AA' in Figure 3a.



b. Along BB' in Figure 3a.

Figure 4. Representative surfacial current density profile (from Liu 1989).

as the distance from the transmitter becomes larger than about one flight height.

The current distribution for the vertical coplanar configuration can be obtained by turning Figure 3a 90° clockwise and considering the flight direction to lie along the new x-axis (i.e., off to the right). The elliptical zone of maximum response would now have its long axis along the flight direction and its short axis perpendicular to this. This means that the vertical coplanar configuration tends to average features encountered along the flight line over a considerably longer distance than does the coaxial configuration, and that it is relatively insensitive to features that lie off to the side of the flight line by more than about one flight height.

The current density in profile from along AA' and BB' in Figure 3a is shown in Figure 4. The dominant response along AA' in Figure 4a is seen to arise from a zone about 1.3 times the flight height in width along the flight line. Side lobes are also present in which the currents actually run counter to their direction in the main zone. Slicing the distribution perpendicular to the flight line along BB' yields the pattern shown in Figure 4b. Here the response is seen to arise primarily from a zone about four flight heights wide.

The vertical coplanar current density profiles can be obtained by simply replacing Figure 4b with Figure 4a. This again demonstrates the reduced resolution along the flight path of about four times less than for the coaxial case.

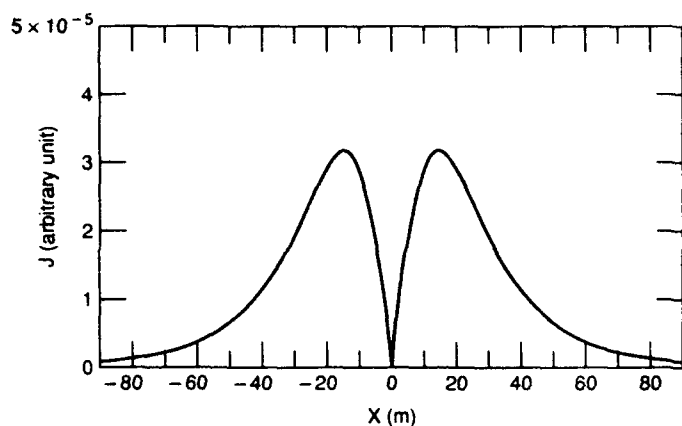


Figure 5. Representative surfacial current density profile along AA' and BB' in Figure 3b (from Liu 1989).

The current density profile for the horizontal coplanar case is shown in Figure 5. Since the current distribution is axially symmetric, profiles AA' and BB' are identical. The null point below the transmitter shows up clearly, as does the peak of the current ring at plus or minus two-thirds the flight height.

HEM FOOTPRINT SIZE

During the course of developing and evaluating HEM technology for the measurement of sea-ice thickness, a number of studies were made to better define the HEM footprint size. An empirical assessment was made by Kovacs et al. (1987), in which a HEM system was flown above a grid area on a multiyear ice floe. Drillhole-measured ice thickness varied from about 2 to 5 m within the grid area. The

drillhole-measured ice thickness was then averaged within a successively enlarged rectangular area under the HEM antenna until the averaged drillhole-measured ice thickness agreed with the value estimated from the measured HEM response. This assessment indicated that for the co-axial coil arrangement the apparent footprint diameter is about 1.25 times the bird's height. Since the shape of the induced current field is definitely not rectilinear and the number of drillhole measurements was limited, this footprint-altitude ratio estimate may not be very accurate.

At about the same time a numerical analysis of HEM footprint size was carried out by Liu and Becker (Becker et al. 1987, Liu 1989, Liu and Becker 1990). In this assessment the fraction of the total HEM response, generated by the induced current flowing at the surface, within a square box centered beneath the transmitting antenna was estimated. The length of the box's sides was varied to estimate the fractional response for different "footprint" sizes for a transmitter situated 30 m above a seawater surface. The footprint estimates for the coaxial and horizontal coplanar modes are shown in Figure 6 (Liu 1989). At the 90% fraction contribution the apparent footprint-altitude ratio is shown to be 1.35 for the coaxial and 3.73 for the horizontal coplanar antenna system. The former is in good agreement with the above assessment of Kovacs et al. (1987). Nevertheless, since the induced current system is definitely not rectilinear, this footprint estimator may also overestimate the footprint-altitude ratio by averaging zones of high current den-

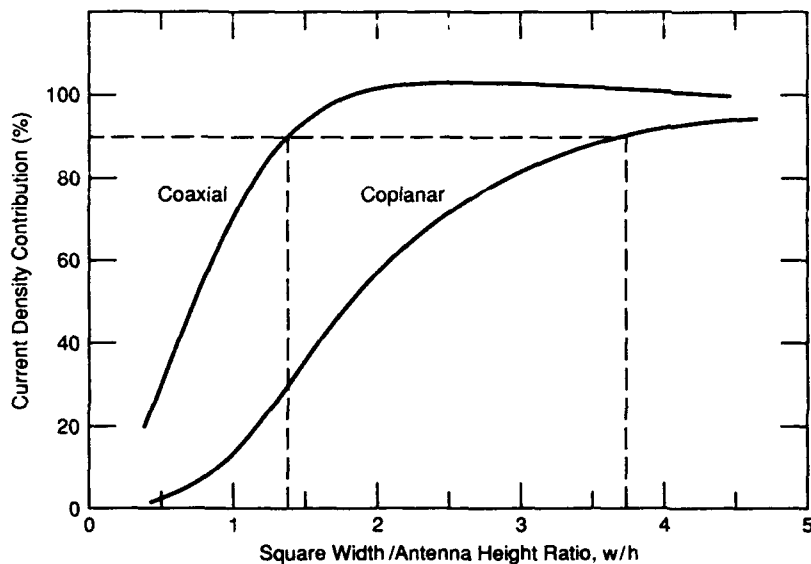


Figure 6. Estimated surfacial current density contribution at a 30-m elevation for a coaxial and a coplanar HEM antenna coil orientation versus an idealized square footprint width to antenna height ratio. Note that for the coplanar coil orientation, about 15% of the measured response can be expected from a box having a width equal to the bird height and about 90% can be expected from a box having a width of 3.7 times the bird height (after Liu 1989).

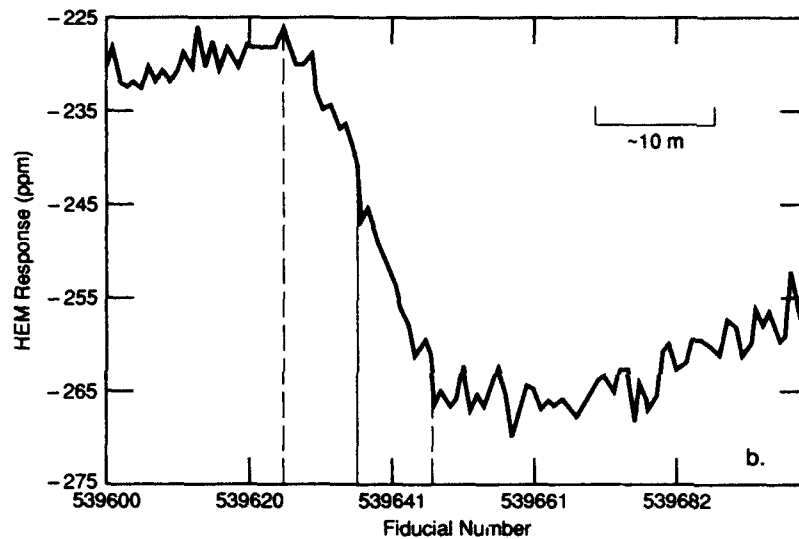
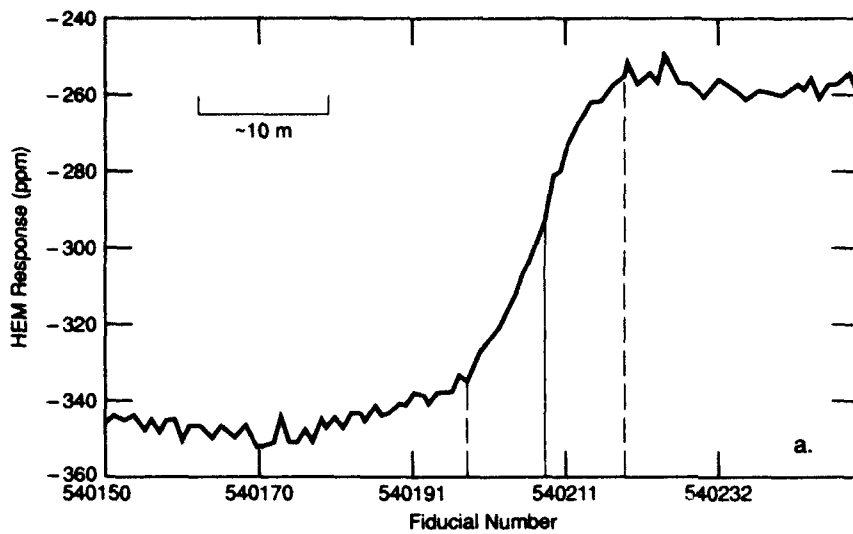


Figure 7. Measured response of a coaxial HEM system flown (a) from over thick first-year sea ice out over a lead with thin ice and (b) from the thin lead ice back over the thicker first-year sea ice.

sity (and therefore contributing to a stronger system response) with zones of much weaker current. Liu (1989) did not calculate an apparent footprint size for the vertical coplanar system, but by examination of the current density profiles and comparison with the existing estimates, a reasonable value would be approximately four times the antenna height.

The wideband HEM induction sounding system was field tested near Prudhoe Bay, Alaska, in April-May 1990. This system could be operated in either a coaxial or a horizontal coplanar mode at a sampling rate of 50 Hz. An example of each mode will be discussed as related to the footprint-altitude ratio. The frequencies used (30 to 100 kHz) were high, so that the majority of the induced current flow occurred near the surface of the seawater.

A site was selected where a step in sea-ice thickness occurred from fairly thick (1.75 m) first-year ice to very thin (0.1 m) lead ice. The HEM-measured

response over this transition was plotted, and the start and end of the HEM response arising from the step change in ice thickness was estimated. This was then compared to the average height of the HEM system and the aircraft speed (65 knots) to estimate the flight distance vs. fiducial number. The raw HEM data were analyzed. No anti-alias filtering or spherical noise removal was performed, although the data were baselined for drift removal and calibrated to read in parts per million. The apparent footprint for each coil configuration was then estimated.

The response of the coaxial system at the first-year/lead ice transition for two overflights is shown in Figure 7. The fiducial width of the transition zone has been marked (dashed line), as has the central position, which represents the location of the first-year ice edge or step in ice thickness. For the data in Figures 7a and 7b the analysis indicates an apparent footprint of 13.9 and 13.2 m, respectively, or 0.8 and

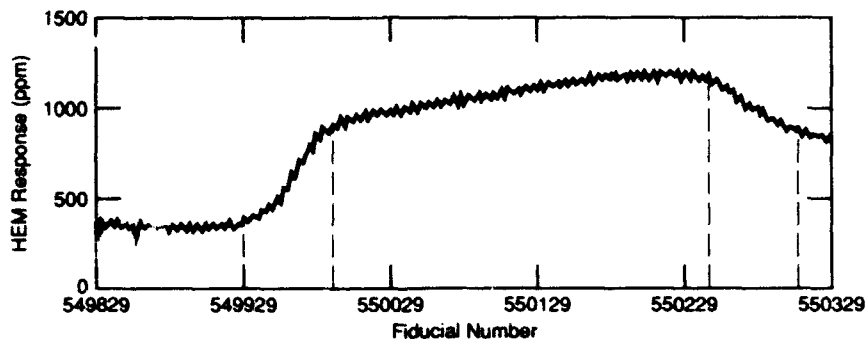
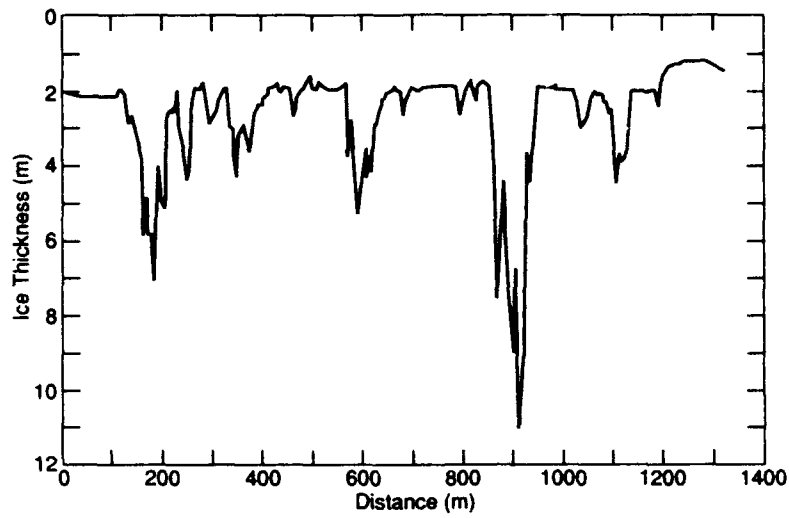
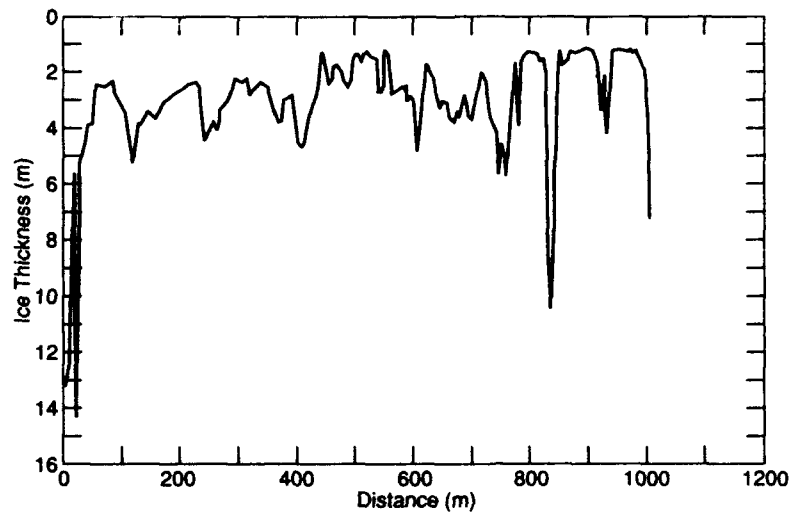


Figure 8. Measured response of a coaxial HEM system as it was flown from over thick first-year sea ice out over thin lead ice and then back over first-year sea ice.



a. 1990.



b. 1991.

Figure 9. Ice thickness distribution along the 1990 and 1991 survey lines.

0.9 times the antenna elevation above the seawater. These values are appreciably less than those determined by Kovacs et al. (1987) of 1.25 and Liu (1989) of 1.35 for a coaxial coil system. However, these low footprint-altitude ratios may be off by up to 20% due to an uncertainty in the GPS-estimated flight speed at the instant of passing over the step area.

The response of a horizontal coplanar coil system flown over a narrow lead is shown in Figure 8. At an estimated flight speed of 65 knots the footprint works out to be approximately 66 m at an average antenna elevation of 18 m above the seawater. This results in an apparent footprint-altitude height ratio of 3.7, which is in agreement with the assessment of Liu (1989) of 3.7 at the 90% response contribution level as shown in Figure 6.

During the 1990 and 1991 HEM sea-ice thickness measurement test and evaluation program, control lines were laid out across the sea ice. The 1990 line was 1.3 km long and extended across first-year sea ice from 1.3-m-thick ice in a lead to 11-m-thick ice in a pressure ridge. The 1991 line was 1.0 km long and crossed both first-year and multiyear sea ice that varied from about 1.6 to 14 m in thickness. Along each line the snow cover plus ice thickness, hereafter called the ice thickness, was determined by drillhole measurements made at 5-m intervals. The drillhole-measured ice thickness along the 1990 and 1991 survey lines is shown in Figures 9. The mean thickness and standard deviation of the ice along the 1990 survey line were 2.65 and 1.48 m, respectively, and for the 1991 survey line they were 3.02 and 1.85 m, respectively.

Two HEM ice-thickness sounding runs were made over the 1990 survey line using the horizontal coplanar coil configuration. The average height of the bird above the seawater during pass 1 was 20.7 m and

for pass 2 it was 22.8 m. The mean and standard deviation for pass 1 were 2.66 m and 1.16 m, respectively, and for pass 2 they were 2.72 and 1.22 m. There is remarkable agreement between the mean drillhole-measured and HEM-estimated ice thickness values. This agreement was a result of the short HEM flightlines, during which time nonlinear system drift was minimal, and the resulting HEM data were therefore of the highest quality. An example of the HEM-estimated ice thickness for pass 1 vs. the drillhole-measured values is shown in Figure 10. Note that the HEM data do not fully reveal the depth of the pressure ridge keels. This is a result of the spatial smoothing of ice relief, which occurs as a result of the wide HEM footprint.

An assessment of the horizontal coplanar coil footprint size was made as follows. The drillhole-measured and the HEM-estimated ice thickness vs. distance along the 1990 survey line were analyzed to reveal the normalized autocorrelation function of ice thickness vs. the lag distance as outlined in Buznev and Dubovtsev (1971) and Rothrock (1986). Of interest is the lag distance at which the autocorrelation function curve has its first zero crossing. This represents the minimum distance between statistically independent ice thickness measurements. For the drillhole measurements and the pass 1 and pass 2 HEM data this distance is about 60, 70, and 80 m, respectively, as shown in Figure 11. A running average of the drillhole data was then made in which the data bin size was progressively increased until the autocorrelation function for the running average data set passed through zero at the same lag distance as the HEM data.

The final bin size resulting from this process provided the number of drillhole measurements and the linear distance along the survey line over which the

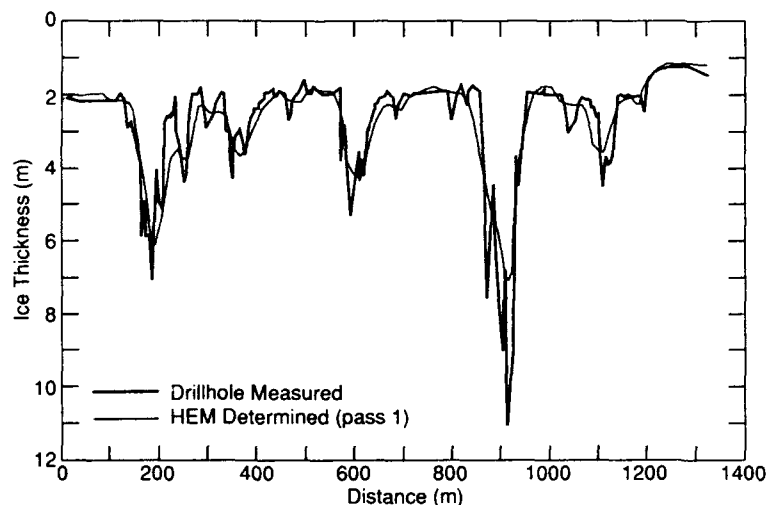
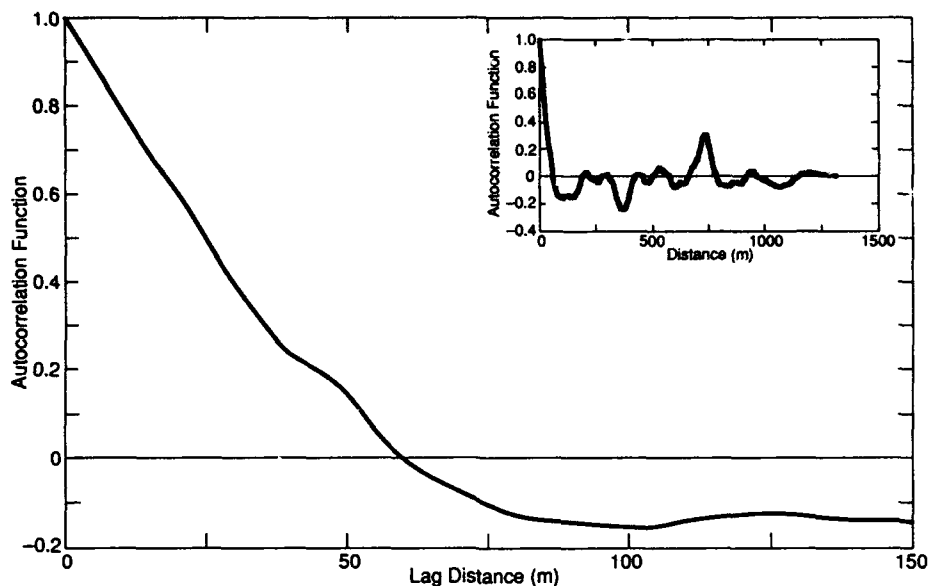
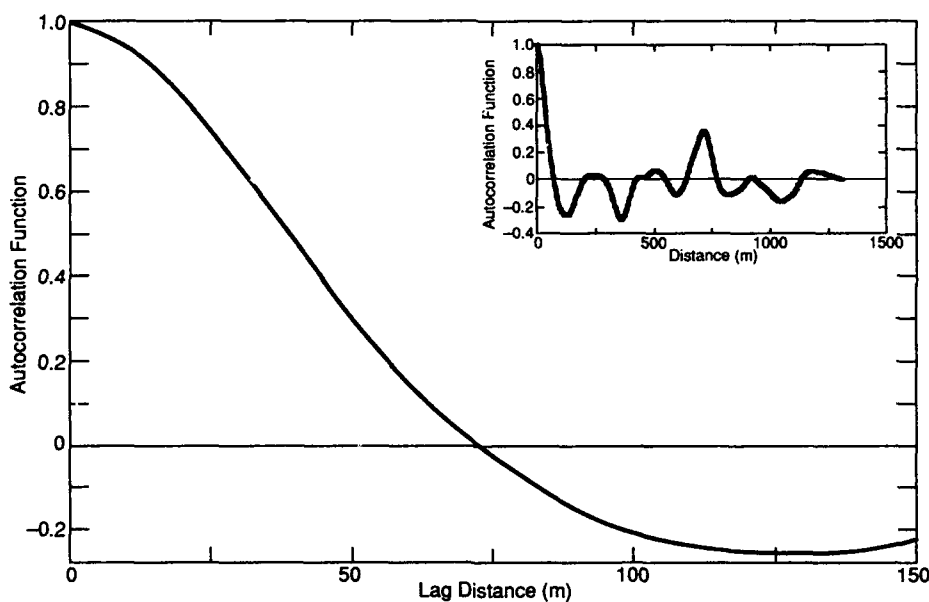


Figure 10. HEM-determined vs. drillhole-measured ice thickness along the 1990 survey line.



a. Drillhole data.



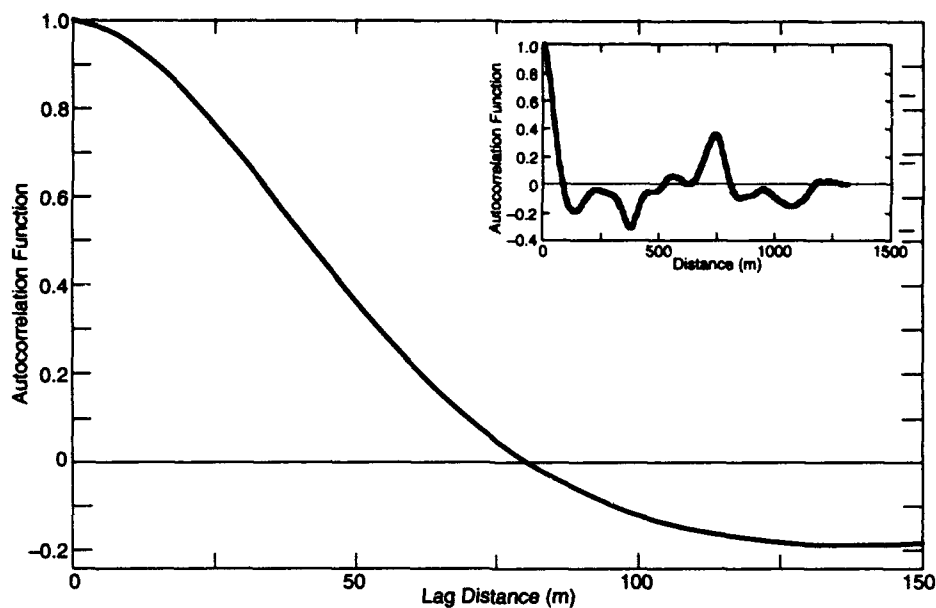
b. Pass 1.

Figure 11. Auto-correlation function of ice thickness vs. lag distance for (a) the drillhole-measured and (b and c) the HEM-determined ice thickness along the 1990 survey line.

measurements were averaged to obtain a zero lag distance comparable to the HEM data. For passes 1 and 2 the distances were 73 and 100 m, respectively. Since the average antenna height above the seawater for passes 1 and 2 was 20.7 and 22.8 m, respectively, the apparent footprint-altitude ratio for each pass was 3.5 and 4.0, respectively.

Three HEM ice-thickness sounding runs were made over the 1991 survey line. The average bird

height during passes 1, 2, and 3 was 23.0, 22.1, and 24.0 m, respectively. The mean and standard deviation for the HEM-estimated ice thickness were: for pass 1, 2.90 and 0.54 m; for pass 2, 2.90 and 0.59 m; and for pass 3, 3.01 and 1.85 m. The agreement between these mean ice-thickness values and those determined from the drillhole-measured data of 3.02 m is very good, for the same reason previously given for the good comparison between the 1990 data sets.



c. Pass 2.

Figure 11 (cont'd).

An example of the HEM-determined ice thickness for pass 2 vs. the drillhole-measured values is shown in Figure 12. While the mean thickness as determined by the HEM system (2.90 m) and the drillhole-measured value (3.02 m) are in good agreement, it is apparent from a comparison of Figures 10 and 12 that more smoothing occurred in the 1991 HEM profile data. This is partly because the average height of the bird above the ice/water interface was 2.6 m more in 1991 than in 1990. The additional flight height translates into a slightly larger footprint (Fig. 6) and thus more spatial smoothing of the ice relief. The ice

thickness variations along the 1991 survey line were also narrower and occurred at a high frequency. Over ice of uniform thickness, the HEM-estimated ice thickness is not dependent on bird altitude and thus footprint size. However, over deformed ice, the HEM-estimated thickness of an individual sea-ice pressure ridge is quite dependent on the bird altitude. At a first-year pressure ridge a distortion of the EM fields occurs due to the block structure and irregular shape of the ice formation. In addition, where the ridge is narrower than the footprint, a 1-D inversion of the EM data does not provide good

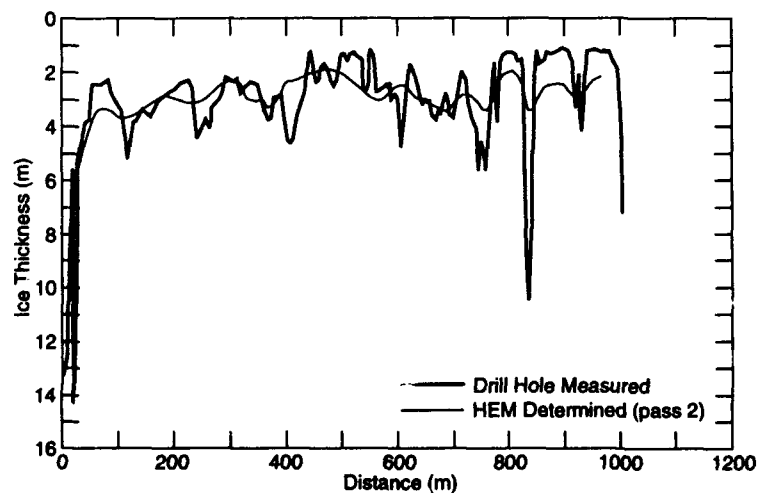


Figure 12. HEM-determined vs. drillhole-measured ice thickness along the 1991 survey line.

draft estimates. These factors affected the HEM-estimated ice thickness profiles, but more so along the 1991 survey line with its narrower ridges.

The effect of bird elevation and therefore footprint size is illustrated in Figure 13, which shows the maximum HEM-determined ice thickness over the thickest ice feature shown in Figure 9a vs. the bird height above the surface for eight sounding passes with the coplanar antenna orientation. Except for the outlier, at the 22.3-m altitude, the data show the decreasing maximum ice thickness trend vs. antenna height relationship that would be expected from the footprint effect. The analysis for the regression line shown passing through the data did not include the outlier, as this data point was collected slightly off to one side of the survey line. The slope of the line in Figure 13 is 0.40 ± 0.12 . This value is in agreement with the value of 0.3 that can be estimated from Liu's (1989) footprint analysis.

As with the 1990 data, a normalized autocorrelation analysis was run on the 1991 data. The results are shown in Figure 14 for the drillhole data and passes 1, 2, and 3. Here the minimum distances between statistically independent samples, as defined by where the autocorrelation function passes through zero, are about 35, 132, 129, and 119 m for the drillhole measurements and passes 1, 2, and 3, respectively. The running average autocorrelation analysis of the drillhole data, as previously described, indicated that zero lag distances or "footprint" lengths of 90, 88, and 70 m, respectively, matched the zero lag distance for passes 1, 2, and 3. The average horizontal coplanar coil antenna heights above the seawater for passes 1, 2, and 3 were 23, 22, and 23.5 m, respectively. Therefore, the apparent footprint-altitude ratio for each pass was 3.9, 4.0, and 3.4, respectively.

The variations in the estimated footprint-altitude ratios may be partly due to bird flight path deviations away from the survey line and to the use of a single line of drillhole ice-thickness measurements to analyze HEM data obtained from the integration of the ice thickness over a much wider swath. Nevertheless, the average of the 1990 and 1991 footprint-altitude ratios is 3.8. This value is in very good agreement with the 3.7 ratio determined by Liu (1989) and can be further verified as follows.

Bergeron and Michel (1986) calculate the footprint of a horizontal coplanar coil pair HEM induction system in the context of the Modified Image Method (MIM) representation of the secondary field. At 50%

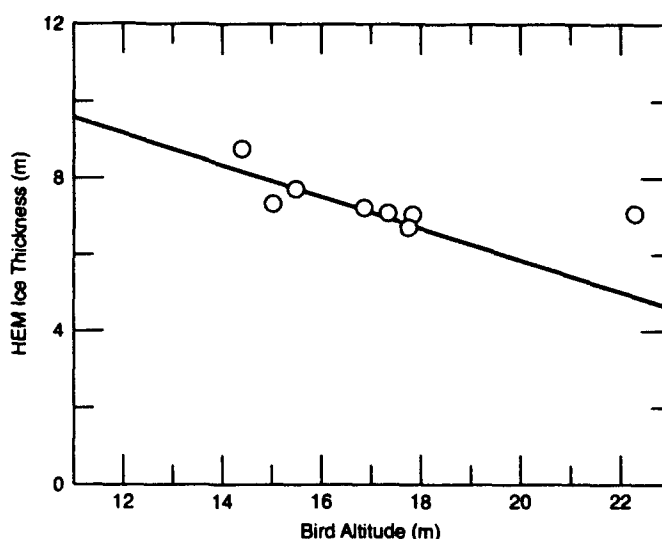


Figure 13. Maximum HEM-determined pressure ridge ice thickness vs. bird elevation above the surface.

of the total signal, the footprint diameter was numerically determined to be twice the altitude. Recently the functional form of a 2-D HEM impulse function for the horizontal coplanar coil configuration was published (Bergeron et al. 1992). The model for the impulse function is the secondary field produced by a line source current induced in the image plane by the primary HEM field. This is the same model used by Liu (1989) except that the surface current sheet is placed one complex screening length below the conducting surface.

The expressions for the normalized line impulse function of the MIM representation of the secondary field for the horizontal coplanar (HCP) and vertical coaxial (VCX) coil configurations are as follows:

HCP:

$$Z_n = \frac{1 + 6r^2}{(1 + r^2)^{3.5}}$$

VCX:

$$X_n = \frac{1 - 1.5r^2}{(1 + r^2)^{3.5}}$$

where

$$r = \frac{x}{h^*}$$

and

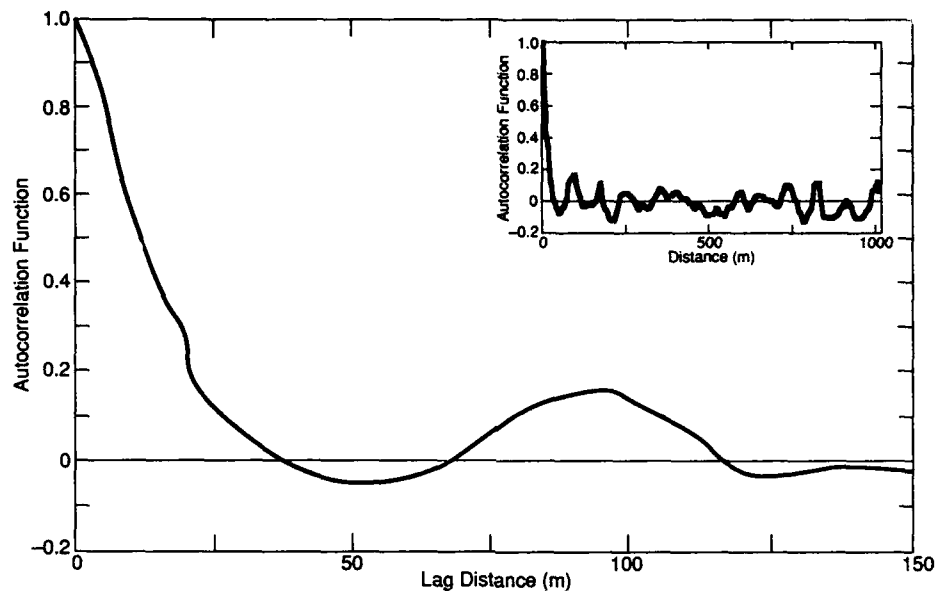
$$h^* = h_{alt} + \delta_{eff}''$$

in which x is the horizontal coordinate of the line

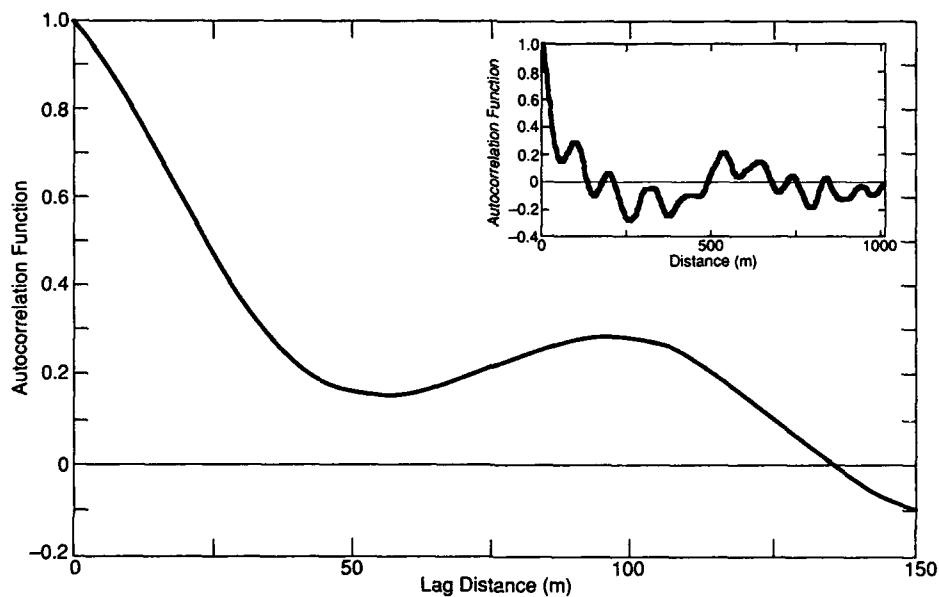
source, oriented in the y direction, h_{alt} is the altitude of the coincident source-receiver coils above the conduction structure, and δ_{eff}^* is the complex effective skin depth of the conducting structure, which makes h^* the complex altitude. Because these expressions contain both the altitude and the effective skin depth, the impulse response can be range-dependent.

From their results we now calculate the width of the 10% line impulse function at 10% of the maximum

value or 90% of total signal level for the HCP coil configuration and find it to be $3.7 h$ where h is the bird altitude. This width is a measure of the 2-D HEM footprint. For the VCX coil arrangement, the calculation of the 10% line width of the 90% 2-D footprint of the HEM impulse function gives a value of $1.32 h$. These results agree with Liu's (1984) and with those derived from field data as presented in this report.

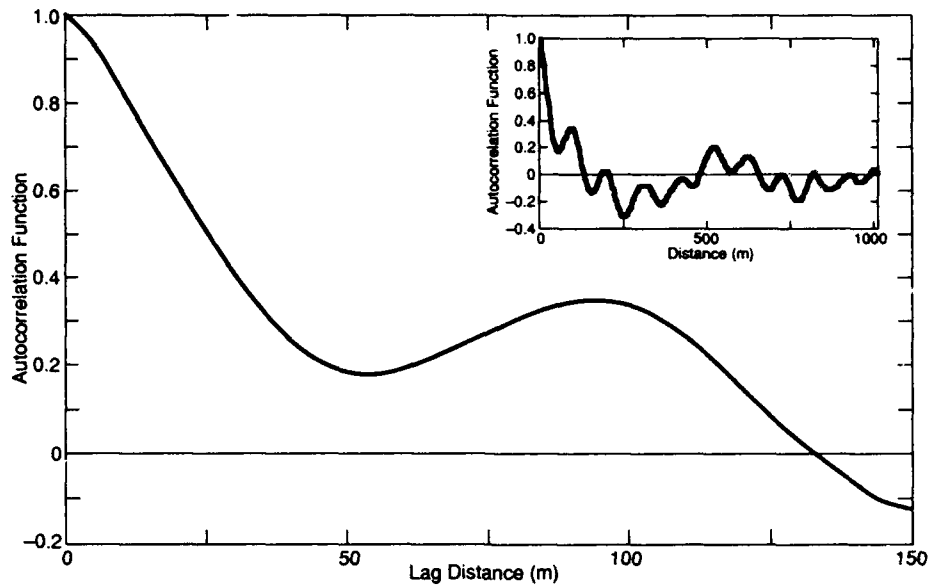


a. Drillhole data.

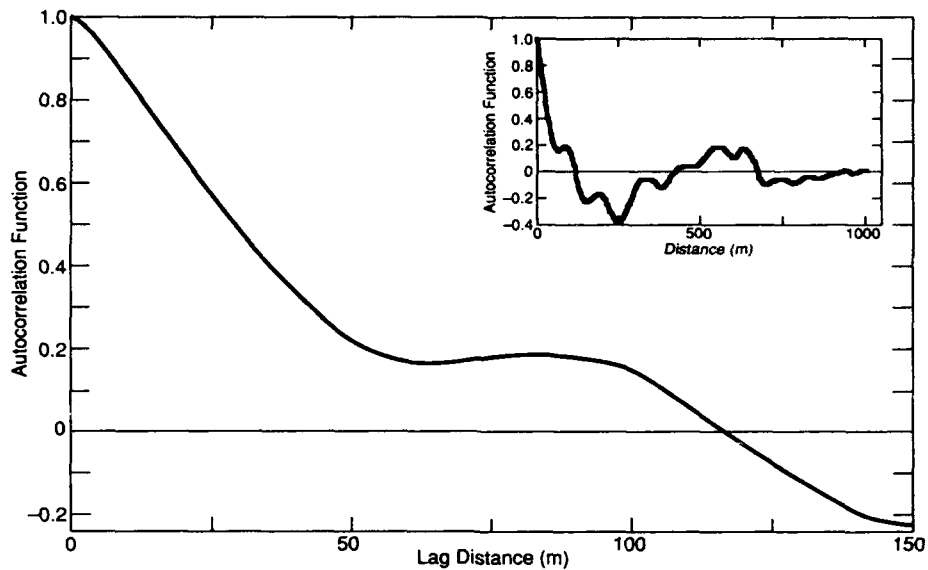


b. Pass 1.

Figure 14. Auto-correlation function of ice thickness vs. lag distance for (a) the drillhole-measured and (b through d) the HEM-determined ice thickness along the 1991 survey line.



c. Pass 2.



d. Pass 3.

Figure 14 (cont'd). Auto-correlation function of ice thickness vs. lag distance for (a) the drillhole-measured and (b through d) the HEM-determined ice thickness along the 1991 survey line.

CONCLUSIONS

In this report assessments are given for the apparent footprint-altitude ratio for coaxial and horizontal coplanar coil HEM sounding systems. The findings indicate that the apparent footprint diameter of a coaxial and a horizontal coplanar HEM system is respectively about 1.25 and 3.75 times the antenna

height above the sea surface and that the smallest HEM footprint is obtained with the use of a coaxial coil arrangement. In principal, this configuration would allow for a better assessment of ridge keel depth and geometry, but not ice volume. However, the reason for not using a coaxial coil configuration is that the signal-to-noise ratio becomes less favorable by a factor of about four.

REFERENCES

- Becker, A., G. Liu and H.F. Morrison (1987)** Airborne electromagnetic sensing of sea ice thickness. University of California, Berkeley, Engineering and Geoscience, Final Contract Report to USA Corps of Engineers, Cold Regions Research and Engineering Laboratory.
- Bergeron, C.J. Jr. and G.A. Michel (1986)** Modified image method applied to AEM coastal surveys. *Journal of Geophysics*, 51.
- Bergeron, C.J. Jr., J.W. Ioup, G.E. Ioup, L.B. Trink, A.M. Amini and A. Kovacs (1992)** Convolution modeling for 1-D inversion of 2-D AEM sea ice data. In *Proceedings, Society of Exploration Geophysics Annual Meeting, 25-29 October*, p. 466-469.
- Buznev, A.Ya. and V.F. Dubovtsev (1971)** Statistical characteristics of some ice cover parameters in the Arctic. In *Proceedings* (N.A. Volkova, Ed.). Arctic and Antarctic Science Research Institute Hydrometeorological Press, Leningrad, 303: 166-179.
- Kovacs, A. and J.S. Holladay (1990)** Sea ice thickness measurement using a small airborne electromagnetic sounding system. *Geophysics*, 55: 1327-1337.
- Kovacs, A., N.D. Valleau and J.S. Holladay (1987)** Airborne electromagnetic sounding of sea ice thickness and sub-ice bathymetry. *Cold Regions Science and Technology*, 14: 289-311.
- Liu, G. (1989)** Airborne electromagnetic sensing of sea ice thickness. Ph.D. thesis, University of California at Berkeley.
- Liu, G. and A. Becker (1990)** Two-dimensional mapping of sea ice keels with airborne electromagnetics. *Geophysics*, 55: 239-248.
- Rothrock, D.A. (1986)** Ice thickness distribution—Measurement and theory. Chapter 8 in *The Geophysics of Sea Ice* (N. Untersteiner, Ed.), NATO ASI Series B: Physics, vol. 146. New York: Plenum Press, p. 551-575.

